Nanoscale

Accepted Manuscript

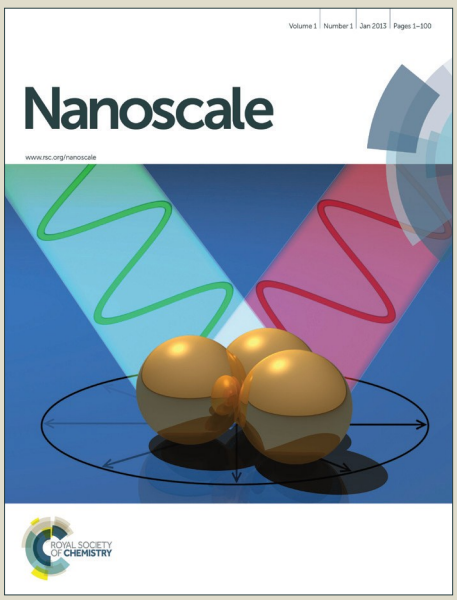

ROYAL SOCIETY OF CHEMISTRY

www.rsc.org/nanoscale

Nanoscale

ARTICLE

Real-Time Label-Free Quantitative Fluorescence Microscopy-Based Detection of ATP Using a Tunable Fluorescent Nano-Aptasensor Platform

Received 00th January 20xx,
Accepted 00th January 20xx

DOI: 10.1039/x0xx00000x

www.rsc.org/

Sajal Shrivastava[a], Il-Yung Sohn[a], Yeong-Min Son[a], Won-Il Lee[a], and Nae-Eung Lee[a,b,c] *

Although real-time label-free fluorescent aptasensors based on nanomaterials are increasingly recognized as a useful strategy for the detection of target biomolecules with high fidelity, the lack of an imaging-based quantitative measurement platform limits their implementation with biological samples. Here we introduce an ensemble strategy for a real-time label-free fluorescent graphene (Gr) aptasensor platform. This platform employs aptamer length-dependent tunability, thus enabling the reagentless quantitative detection of biomolecules through computational processing coupled with real-time fluorescence imaging data. We demonstrate that this strategy effectively delivers dose-dependent quantitative readouts of adenosine triphosphate (ATP) concentration on chemical vapor deposited (CVD) Gr and reduced graphene oxide (rGO) surfaces, thereby providing a cytotoxicity assessment. Compared with conventional fluorescence spectrometry methods, our highly efficient, universally applicable, and rational approach will facilitate a broader implementation of imaging-based biosensing platforms for the quantitative evaluation of a range of target molecules.

Introduction

The vast majority of biological and biomedical studies on the molecular and cellular levels rely on imaging to acquire information on the specific cellular responses to factors such as chemical agents, mechanical stress, and genetic modifications. In most imaging approaches, observation and image acquisition are entirely visualization-oriented. However, several aspects of the resultant images can often be quantified using processing software. In particular, fluorescence microscopy has been widely used to determine the quantitative localization of target molecules in living cells[1-3], to study the dynamics of biomolecules during biochemical reactions,[4,5] and to measure the specific interactions of cellular macromolecules.[6] To these ends, various techniques such as fluorescence photobleaching-based analysis,[7,8] fluorescence resonance energy transfer (FRET),[9,10] and fluorescence lifetime imaging[11,12] have been developed. These techniques have become indispensable for *in vitro* and *in vivo* studies. While numerous fluorescence microscopy-based methods for quantifying the levels of target proteins have been developed, these methods have not yet achieved sufficient accuracy and sensitivity to enable the determination of molecule concentrations from fluorescence intensities. Current methods also have not yet achieved absolute quantitative analysis as an integral part of a biosensing system. Generally speaking, fluorescence spectrometry has predominantly been used to quantify biologically important molecules.

For these reasons, a fluorescence imaging-based platform enabling the real-time quantitative monitoring of receptor-target interactions has the potential to be a novel and powerful bioanalytical tool. The development of such a fluorescence imaging-based quantitative technique requires receptors such as antibodies, enzymes, and aptamers that specifically bind to the desired target analytes. These receptor-target interactions can be quantified by the changes in fluorescence intensity upon binding. In particular, short oligonucleotide aptamers have become a very significant molecular tool for quantitative diagnostics.[13] Compared with biosensors developed using other receptors such as antibodies and enzymes, aptamer-based biosensors offer unprecedented benefits for the analysis and quantification of a wide range of target molecules.[14] Considering the high specificity and affinity of aptamers for a large number of targets ranging from small molecules[15] to large proteins[16,17] and even cells,[18,19] the integration of quantitative fluorescence microscopy (QFM) with an aptamer-based biosensing platform has the potential to provide a simple, powerful, and versatile approach. This integration also promises to extend the capability of imaging from qualitative to quantitative analysis. The development of an effective imaging-based aptasensor platform requires receptor immobilization, which yields better spatial distribution and improved aptamer stability over a range of factors such as ionic strengths, pH, and temperatures.[20,21] Receptor immobilization can be achieved with large-area high quality monolayered two-dimensional (2D) nanomaterials such as graphene (Gr) and reduced graphene oxide (rGO). However, current fluorescent aptasensors, particularly those based on carbon nanomaterials, are not yet suitable for use in imaging-based quantification techniques. The fluorescent aptasensors developed so far utilize fluorescent dye-labeled aptamers; therefore, their

[a] School of Advanced Materials Science & Engineering, Sungkyunkwan University, 2066 Seobu-ro, Jangan-gu, Suwon, Gyeonggi-do 16419, Korea
[b] SKKU Advanced Institute of Nanotechnology (SAINT), Sungkyunkwan University, 2066 Seobu-ro, Jangan-gu, Suwon, Gyeonggi-do 16419, Korea
[c] Samsung Advanced Institute for Health Sciences & Technology (SAIHST), Sungkyunkwan University, 2066 Seobu-ro, Jangan-gu, Suwon, Gyeonggi-do 16419, Korea. E-mail: nelee@skku.edu
*E-mail: nelee@skku.edu
Electronic Supplementary Information (ESI) available: See DOI: 10.1039/x0xx00000x

covalent immobilization complicates signal detection due to the high quenching capabilities of these carbon nanomaterials.[22,23] In addition, fluorescent dye labeling of aptamers is expensive, tedious, and often involves multiple chemical reactions. Moreover, fluorescent dye labeling can also alter aptamer stability and selectivity.[24] Therefore, appropriate label-free fluorescent aptasensors must be developed. The integration of such covalently attached aptasensors with a signal amplification strategy is a promising approach for an imaging-based platform enabling highly accurate and precise quantitative fluorescence evaluation.

Label-free quantitative measurements with signal amplification can be achieved with intercalating dyes such as SYBR Green-I (SGI), which binds specifically and robustly to double-stranded deoxyribonucleic acid (dsDNA) molecules.[25] This intercalating dye has shown temperature stability which enables it to be commonly used in quantitative polymerase chain reaction within a range of temperature and is also stable within physiological pH limits at which biomolecular detection and quantification have been typically performed. Additionally, the SGI has also shown selectivity for double-stranded aptamer-complementary DNA (cDNA) complexes with high sensitivity which makes it suitable for biomolecular detection and quantification.[26] Furthermore, SGI intercalation with double-stranded aptamer complexes is a simple (one step), robust, and reliable procedure for quantifying biomolecules. This label-free strategy also has the potential to enable real-time monitoring, both qualitatively and quantitatively, of analyte-aptamer interactions.

Herein, the feasibility of an imaging-based platform for the quantitative assessment of therapeutic responses is demonstrated. Specifically, a label-free fluorescent nano-aptasensor was used in combination with QFM to detect and quantify adenosine triphosphate (ATP), the energy currency of cells that is essential for the execution of various functions in living organisms. The aptasensor consisted of SGI-intercalated aptamer complexes that were covalently immobilized on Gr and rGO, thus enabling qualitative and quantitative measurements of ATP. The aptasensor was also shown to exhibit length-dependent increases in fluorescence intensity and hence provides a tunable platform for biomolecule quantification. Since the sensor relies on the specificity of the interaction between the aptamer and its target molecules, this platform promises to be widely applicable to the quantification of a number of targets including ions, small biomolecules, proteins, and even cells.

Results and Discussion

Design scheme and strategy for label-free quantification

In this study, our aims were to calibrate a QFM workflow and to use this technique to detect various concentrations of ATP in biological samples. Our workflow was designed for label-free quantitative detection using Gr and rGO aptasensors. A schematic representation of the SGI-based label-free aptasensor is shown in **Figure 1**. SGI intercalates specifically into the dsDNAs with a very low background. The intercalated dsDNAs were covalently immobilized on rGO and Gr, which provide higher fluorophore counts compared with fluorescein amidite (FAM)-labeled aptamers. Previous Gr-based and rGO-based fluorescence detection strategies have demonstrated that labeling is essential for fluorescence-mediated detection of target molecules on the surfaces of these two substances.[27-29] Aptamer desorption from the Gr or rGO surface can occur even without an interaction between the aptamer and its target molecule, which limits the accuracy of detection and quantification of biomolecule concentration.[21] For optimal stability and efficiency of biomolecule-aptamer interactions in the context of fluorescent aptasensors, the immobilization of dsDNAs on Gr and rGO using 1-pyrenebutanoic acid succinimidyl ester (PBASE) as a linker molecule appears to be the most effective strategy. This approach protects the dsDNAs from external cues and provides a fundamentally more stable platform for biomolecule detection. Hence, the covalent immobilization of aptamers used in this study results in higher accuracy of biomolecule quantification compared with other approaches. Moreover, considering the quenching properties of rGO and Gr, the aptamer complex will have significantly greater fluorescence emission compared with the fluorescence emission from the FAM-labeled aptamer duplex. In the absence of ATP, the aptamer complexes on the Gr and rGO surfaces exhibit strong fluorescence. In contrast, as the concentration of ATP increases, free ATP binds to the dsDNA-aptamer complex, causing the release of cDNA. This dissociation results in a significant reduction in the fluorescence intensity due to the release of SGI into the solution.

It is apparent that our imaging-based quantitative aptasensing method relies on the change in mean fluorescent intensity due to the release of SGI from aptamer complexes; hence, the concentration of SGI used to prepare these complexes can affect the performance. In this regard, the aptamer duplexes were incubated with various concentrations of SGI until the optimal fluorescence intensity was achieved. An increment in fluorescence intensity was observed up to an SGI concentration of 485 nM for Ap1 and Fap aptamer duplexes. On the other hand, the optimal fluorescence intensity for Ap2 was attained at 738 nM SGI in the absence of ATP. Based on these observations, those concentrations were used in subsequent experiments. Therefore, quantitative microscopy-based analysis of ATP can be realized by optimizing the SGI concentration and then observing the fluorescence intensity change of SGI on each surface.

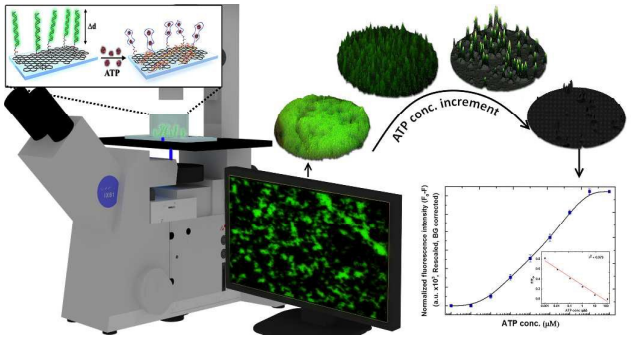

Figure 1. Schematic representation of the label-free fluorescence-based strategy for ATP quantification using Gr, rGO, and SGI-intercalated aptamers. A tunable fluorescence platform was developed using SGI-intercalated dsDNAs (aptamer complexes) with controlled lengths (Δd). The binding of two ATP molecules to each aptamer induces a conformational change in the dsDNA, leading to the release of SGI and cDNA from the SGI-intercalated dsDNA. The changes in fluorescence intensity are measured by quantitative fluorescence microscopy (QFM) both before and after the addition of various concentrations of ATP. These images were processed and their mean fluorescence intensities recorded in order to quantify the levels of ATP.

Processing of fluorescence signals for ATP quantification

We validated the potential of our imaging-based aptasensing strategy to quantify small biomolecules in biological samples. As described in detail in the Materials and Methods section, the aptasensors were assigned to control, nontreated (NT), and experimental groups before the addition of various concentrations of ATP. The control group (equivalent to the "blank" in spectrometry) establishes the lower limit of ATP quantification, while the NT group defines the upper limit of fluorescence intensity. The images acquired from the control group did not exhibit any significant background signal; hence, the ATP activity images have excellent *signal*-to-*background* ratios. The background noise during aptasensing on glass substrate modified with aptamer complexes was obtained and compared with that of the Gr and rGO aptasensors immobilized with aptamer complexes. As seen in **Figure S1**, it is very apparent that aptasensing on the glass involved a higher background signal, which implies that the sensing results can be biased and affect the accuracy of quantitative measurements due to higher noise. Moreover, the Gr and rGO aptasensors also show a high binding capacity, aptamer uniformity, and stability of aptamer complexes.

After analyzing the background noise, the fluorescence distribution images on Gr and rGO were acquired at low magnification for a range of ATP concentrations. Images were obtained from each well with one fluorescence channel. In this manner, a large pool of image sets corresponding to ATP-aptamer interactions can be rapidly obtained. These images were then processed to establish the relationship between aptamer length, nanomaterial quenching effect, and background signal by normalizing the fluorescence signals. For this purpose, the raw fluorescence intensity of each image was converted to a normalized fluorescence intensity (F_o-F), where F represents the fluorescence intensity at a given concentration and F_o represents the initial fluorescence intensity before the addition of ATP. Initially, 5 images were collected and the extracted fluorescence intensities were plotted against time to analyze the time required for ATP-aptamer interactions. The aptasensors were incubated with 100 µM ATP, images were acquired at 5 min intervals for 30 min, and the resultant changes in fluorescence intensity were measured (**Figure 2**). As shown in **Figure 2a**, most of the fluorescence changes occurred during 5-20 min, with the fluorescence intensity stabilizing after 20 min. Moreover, enhanced fluorescence was observed on the Gr aptasensor immobilized with the Ap1 complex (see Table 1 for the aptamers used in each experiment) compared with the rGO aptasensor assembled with the identical aptamer. A similar trend was observed with the Ap2 complex (**Figure 2b**), in which the fluorescence intensity reached saturation after 20 min. Thus, increasing the aptamer length resulted in a dramatic increase in fluorescence intensity that stabilized after 20 min for both aptamers. Importantly, increasing the aptamer length did not interfere with the ATP-aptamer interaction, as assessed by the fluorescence signal.

After optimizing the time required for the saturation of ATP-aptamer interaction, the acquired raw fluorescence images were processed to extract the quantitative properties of the fluorescence signals and enable the accessible presentation of this information. The workflow for ATP quantification on Gr and rGO surfaces immobilized with SGI-intercalated aptamers of different lengths is depicted in **Figure 3**. The aptamer distribution patterns on Gr were analyzed and redrawn as 3D interactive plots of fluorescence distribution for the selected ATP concentrations. As shown in **Figure 3a**, the fluorescence distribution patterns indicated that the aptamers were uniformly immobilized on the Gr surface and that the fluorescence intensity decreased with increasing ATP concentration, as expected. To further establish the relationship between ATP concentration and the change in fluorescence intensity, a calibration curve was generated. As shown in **Figure 3b**, the normalized fluorescence intensity of the Gr-Ap1 complex increased with increasing ATP concentrations after 20 min of incubation (r^2 = 0.996). The plot of fluorescence intensity versus ATP concentration presented a typical sigmoidal curve; moreover, the change in normalized fluorescence intensity became saturated just before the ATP concentration reached 100 µM. Most importantly, the relative fluorescence intensity decrease ($\Delta F/F_o$) plotted against the logarithmic value of the ATP concentration was linear from 0.001 µM to 100 µM (the inset of **Figure 3b**), which means that ATP-aptamer recognition can be monitored by fluorescence intensity changes within this range. As shown in the inset of **Figure 3c**, a similar detection limit was observed with the Gr-Ap2 complex. However, the Gr-Ap2 complex exhibited a higher normalized fluorescence intensity (fluorescence enhancement) than the Gr-Ap1 complex (r^2 = 0.995). As shown in **Figure 3d**, the normalized fluorescence intensity of the rGO-Ap1 complex was lower than that of the Gr-Ap1 complex. However, the rGO-Ap1 complex exhibited a similar linear range of detection (r^2 = 0.970) over ATP concentrations ranging from 0.001 µM to 100 µM (the inset of **Figure 3d**). A similar trend was observed with the rGO-Ap2 complex (**Figure 3e**). Specifically, the fluorescence intensity was lower than that of the Gr-Ap2 complex but higher than that of the rGO-Ap1 complex over a similar linear range of detection (the inset of **Figure 3e**). The differences between the aptasensors (Gr and rGO with either Ap1 or Ap2) were highly significant ($p<0.0001$) and the correlation coefficients of the standard curves were always higher than 0.9. The high fluorescence intensities observed in our proposed method may be attributed to the longer aptamers that can presumably bind with more fluorophores than the shorter aptamers. Hence, aptamer length strongly influences fluorescence signal detection. Furthermore, the results also indicated that the rGO aptasensors exhibited a higher quenching efficiency compared with Gr aptasensors. Hence, these results indicate that choice of carbon nanomaterials and aptamer length can enable the tuning of imaging-based quantification without compromising the detection limit. To verify that the enhanced fluorescence was due to the increased aptamer length, the ATP concentration-dependent changes in fluorescence intensity were analyzed by standard spectrometry methods. As shown in **figure S2**, the Ap2 complex showed enhanced fluorescence compared with the Ap1 complex. Consistent with our previous results, increasing the ATP concentration decreased the fluorescence intensity. These results demonstrate that our sensing strategy is capable of universal detection in a label-free manner.

As mentioned earlier, the accuracy of aptasensing is defined by the signal-to-noise ratio and minimum detectable quantity of the analyte. Hence, to demonstrate the sensitivity, the designed imaging-based Gr and rGO aptasensing platforms were compared with the quantitative capability of glass substrate. Following aptamer complex immobilization, the glass substrates were incubated with ATP at concentrations ranging from 10 pM to 1000 µM. As shown in the **Figure S3**, detection using our quantitative fluorescence microscopy method demonstrated that the Gr and rGO aptasensor platforms had three-fold higher sensitivity than the glass substrate. As shown in **Figure S3a**, the normalized fluorescence intensity of the glass-Ap1-complex increased with increasing ATP concentration after 20 min of incubation. However,

it is very evident that the glass substrate displayed a detection limit of 0.1 µM due to a poor signal-to-noise ratio (SNR) compared to those of Gr and rGO aptasensors, which exhibited an improved sensitivity of ATP detection with a detection limit of 0.01 nM. As shown in **Figure S3b**, the glass substrate immobilized with Ap2 complex presented a detection limit similar to Ap1-complex. However, as seen in Gr and rGO aptasensors, a change in aptamer length showed fluorescence enhancement on the glass substrate. As the signal increased, however, the relative noise level also increased, illustrating that glass is inappropriate for use as a tuneable platform. This verifies that the change in fluorescence signal became increasingly more precise due to the quenching capability of these carbon nanomaterials, which increase the fluorescence signal relative to the noise level. Therefore, combined with the advantage of no autofluorescence in the SGI excitation/emission region, better signal-to-noise ratios of Gr and rGO aptasensors offer vastly improved sensitivity for quantification of biomarkers in biological cultures. Hence, the glass-based aptasensors immobilized either with Ap1 or Ap2 were inferior to the Gr and rGO aptasensors.

Additionally, to establish the sensitivity of our imaging-based quantitative method and to confirm that each aptamer-ATP interaction could account for the changes in mean fluorescence intensity during quantification, our system was verified with grid placement, where the system divides the total image area into various small segments (pixels). The pixels spatially sample the change in ATP-aptamer interaction, such that each pixel epitomizes a distinct fixed area in a specific location on the aptasensor. After acquisition of the digital images of ATP binding to aptamers at various concentrations, the fluorescence intensity at each pixel was calculated. For this purpose, the computer-generated datasets of multiple images with known ATP concentrations were used to first determine the minimum region of interest (ROI) necessary to obtain accurate and precise estimates of fluorescence intensities. As soon as the grid was overlaid, the changes in the fluorescent signals of these areas of the image datasets obtained pre- and post-ATP treatment were quantified. The spatial distribution of ATP-aptamer interaction, as shown in **Figure 3a**, the reduction in intensity value changes from one image to the next. For any sample size, it was observed that the mean fluorescence intensity calculated by overlaying the grid at various locations was sequentially decreased with change in ATP concentration. The method generated precise measurements over the entire range of aptamer densities. Thus, this imaging-based aptasensor is not biased by high-density aptamer conditions with relatively ultra-low background noise. We also found that the fluorescence signal intensity was directly proportional to dsDNA length, which means that the biomolecule detection platform can be tuned by modulating the aptamer length. The image processing results and calibration curves revealed a substantial degree of linearity between the relative fluorescence intensity and the ATP concentration. The calibration curve obtained from the analysis of many images indicated that wide-field microscopy measurements are quantitative, since they exhibited a linear response to different ATP concentrations.

The selection of nanomaterial depends on the observed SNR during aptasensing while using a wide-field microscopy. Similarly, the length of aptamer can be adjusted according to the detection limit. The combination of higher SNR and low detection limit defines the accuracy and precision in our imaging-based quantitative aptasensing method. In this study, the magnitudes of the normalized fluorescence intensities were higher on Gr than on rGO; moreover, a higher signal was achieved with a longer aptamer complex (Ap2) than with a shorter aptamer complex (Ap1). The results obtained with the Gr and rGO aptasensors with different aptamer lengths revealed that the linear response was sustained and also demonstrated similar relative fluorescence scales upon normalization. The plots of the relative fluorescence changes reflect variations in the quantitative relationship between fluorescence intensity and ATP concentration. Thus, the similar slopes obtained with both aptamers indicate that our image processing method conserves the relative relationship between fluorescence intensity and ATP concentration for quantitative detection.

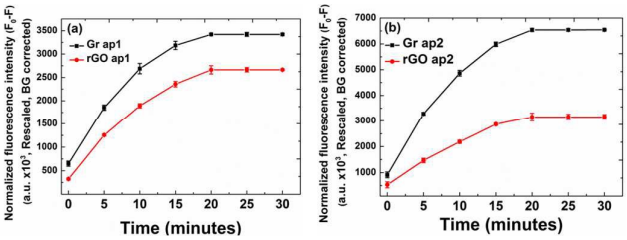

Figure 2. Analysis of ATP-aptamer interactions. Fluorescence intensity changes (Fo-F) were obtained at 5 min intervals in the presence of 100 µM ATP and plotted over time. The fluorescence stabilized after 20 min for (a) Gr as well as (b) rGO immobilized with either Ap1 or Ap2.

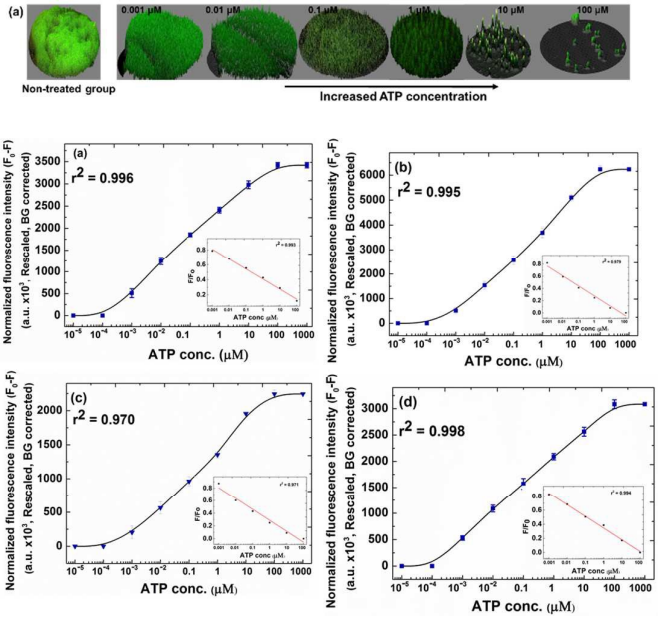

Figure 3. ATP quantification on Gr and rGO surfaces immobilized with SGI-intercalated aptamers of different lengths. (a) Interactive 3D surface plot of the changes in fluorescence intensity at various concentrations of ATP. Images were first acquired for the nontreated (NT) group before any ATP was added. The normalized changes in fluorescence intensity (F-Fo) were recorded for aptamers of different lengths and for different 2D carbon nanomaterials. Different concentrations of ATP were quantified on (b) a Gr-Ap1 aptasensor, (c) a Gr-Ap2 aptasensor, (d) an rGO-Ap1 aptasensor, and (e) an rGO-Ap2 aptasensor. The insets in (b), (c), (d), and (e) indicate the changes in the normalized signal (F/Fo) as the ATP concentration is varied. All data were expressed as mean ± SEM.

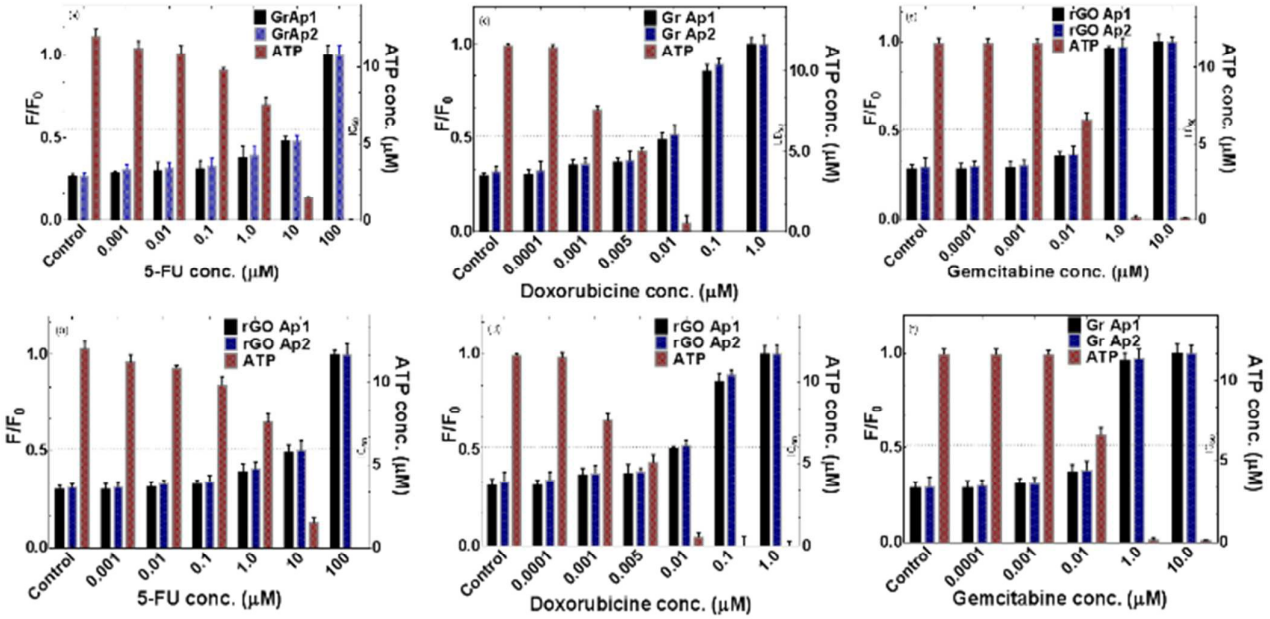

Figure 4. Imaging-based quantitation of ATP using the Gr and rGO aptasensors after the addition of cytotoxic drugs to HeLa cells. The relative fluorescence intensity, F/Fo, and the corresponding ATP concentration are shown for each drug treatment condition. ATP was quantified on the Gr aptasensor with either Ap1 or Ap2 after exposure of cells to (a) 5-fluorouracil, (c) doxorubicin, or (e) gemcitabine. Similarly, ATP was quantified after exposure of cells to (b) 5-fluorouracil, (d) doxorubicin, or (f) gemcitabine. The dotted line represents the IC50 range; all data were expressed as mean ± SEM.

Validation of ATP quantification in a drug-induced cytotoxicity assay

After establishing a calibration curve, it is imperative to validate the ability of the assay to generate quantitative data for unknown samples. We validated our aptasensing methodology by evaluating the relationship between drug exposure, ATP depletion, and cytotoxicity. Hence, our imaging-based quantitative measurement platform was applied to quantify ATP as an index of cytotoxicity in drug-treated cells. The rescaled fluorescence values were then appropriately combined with the average ATP concentrations, which were calculated from the Gr and rGO aptasensors immobilized with the Ap1 and Ap2 aptamer complexes. Next, cell viability was calculated as the quotient of ATP to total fluorescence signal. This aptasensing approach was used to evaluate the efficacy of a number of commercially available generic anticancer drugs against HeLa cells in an *in vitro* assay. The cytotoxic responses of HeLa cells to three well-characterized oncology drugs are shown in **Figure 4**. Noticeable cytotoxic responses to the drugs were reflected in the image data and were also apparent in the $\Delta F/F_0$ values and ATP concentrations. These latter two values were chosen metrics for the treatment response. As shown in **Figure 4a**, F/F_0 reached ~1.0 for both aptasensors at 100 μM 5-fluorouracil (5-FU). Thus, no detectable ATP was released, indicating that >99.9% of the cells were killed after continuous drug exposure. The rGO aptasensor (**Figure 4b**) exhibited a similar trend when the relative fluorescence intensity was plotted against the ATP concentration. For both the Gr and rGO aptasensors, the average ATP concentration reached 7.55±0.861 μM after exposure to 1 μM 5-FU, which corresponds to a 36% reduction in cell viability. In contrast, an 87% reduction in cell viability was observed with 10 μM 5-FU with an average ATP concentration of 1.55± 0.082 μM. Our results indicate that 5-FU reduces cell viability in a dose-dependent manner and that the concentration required to kill 50% of the cells (IC_{50}) ranges from 1-10 μM. To evaluate the sensitivity of this approach, a comparative cytotoxicity analysis was performed between imaging-based and spectrometry-based ATP quantification methods. As shown in **Figure S4a**, treatment with 5-FU resulted in a 50% reduction in cell viability at concentrations ranging from 1-10 μM.

A similar trend was observed for both aptamers, thereby recapitulating the results obtained with the Gr and rGO aptasensors. As shown in **Figure 4c** and **d**, only 0.02% of all HeLa cells survived after exposure to 1 μM doxorubicin and a 50% reduction in ATP concentration was observed at concentrations ranging from 0.001 to 0.005 μM. These results indicate that doxorubicin treatment greatly decreases cell viability; hence, the ATP concentrations were also measured by spectrometry. As shown in **Figure S4b**, treatment with doxorubicin (0.005 μM) caused a 58.4% reduction in the ATP concentration (5.186± 0.466 μM); moreover, the observed IC_{50} value of doxorubicin ranged from 0.001 to 0.005 μM. Thus, the average ATP concentrations and cell viabilities obtained using the spectrometry-based method were highly comparable with those obtained with the Gr and rGO aptasensors. The cytotoxic effect of gemcitabine was also examined by measuring the fluorescence intensities from the rescaled images. As shown in **Figure 4e**, HeLa cells cultured in the absence of gemcitabine contained up to 11.59± 0.869 μM ATP as measured by the Gr aptasensor. A similar trend was observed with the rGO aptasensor (**Figure 4f**), for which the average ATP concentration as quantified by Ap1 and Ap2 was 11.51 ± 0.672 μM. This value is highly comparable with that of the Gr aptasensor. Moreover, gemcitabine exhibited dose-dependent cytotoxicity in HeLa cells. Specifically, the relative fluorescence intensity started at 0.289± 0.033 and increased to 1.0 when cells were exposed to 10 μM

gemcitabine, while the ATP concentration decreased from 11.5 µM to below the limit of detection. These experiments revealed that our assay was able to establish a linear relationship between the drug concentration and the relative fluorescence intensity. As shown in **Figure S4c**, according to the spectrometry-based method the ATP concentration decreased from 12.59 ± 0.564 µM to 6.48 ± 0.895 µM when cells were incubated with 0.01 µM gemcitabine. This trend was similar to that seen with our Gr and rGO aptasensors.

Overall, the wide-field microscope images of ATP-aptamer interactions after exposure of cells to 5-FU, doxorubicin, or gemcitabine (or a nontreated control) indicate that these drugs can reduce cell viability. Specifically, treatment with these drugs resulted in increased relative fluorescence intensities, indicating that the cellular ATP concentrations were decreased. This method thus provides a simple and rapid means for reporting fractional inhibitory concentrations; furthermore, our method was validated by spectrometry-based measurements of ATP concentrations after drug treatment. It is evident that the ATP concentrations calculated from the calibration curve revealed similar patterns of drug cytotoxicity to those obtained with spectrofluorometry methods. Therefore, based on these data, our imaging-based label-free aptasensing approach is an attractive alternative to conventional assays for the fast and reliable quantitative evaluation of drug cytotoxicity. Since our approach is imaging-based and quantitative, it can also be integrated with other cell imaging results to obtain viability statistics and to quantify the extent of heterogeneity in the treatment response.

Moreover, our strategy omits the need for labeling protocols, which can lead to false positive signals, are cost-intensive to develop, and exhibit limited selectivity compared with other fluorescent aptasensors that require dual-labeling of aptamers with molecular beacons[30-33] or fluorophore donors and acceptors.[34,35] Our system not only overcomes technical barriers to use standard spectrometry methods for the detection of biomolecules on nanomaterials in a non-solution form, but also provides qualitative and quantitative information about the interaction that is typically not achieved in conventional assays. Furthermore, our strategy amplifies the signal several fold, which facilitates fluorescence detection. Previous studies using fluorescent dye-labeled aptamers covalently immobilized on nanomaterials such as Gr and rGO have revealed that the quantitative detection of small molecules in biological samples by fluorescence microscopy is complicated by the high quenching capabilities of these materials and the insufficient detection limit of most wide-field microscopes. Importantly, fluorescence measurements have shown that tight DNA binding coupled with long dsDNA molecules yields substantially higher intensities than those achieved with labeled aptamers on Gr and rGO surfaces. Due to the increased fluorescence quenching on Gr and rGO, our SGI-based signal amplification strategy not only yields a signal suitable for biomolecular detection, but also offers a label-free sensing platform. The binding of ATP and other molecules to their cognate aptamers is reversible.[36] Hence, the key advantage of this label-free strategy is the ease by which aptasensors can be generated and regenerated. Thus, this label-free aptasensing strategy offers a reusable platform for the quantification of various analytes. Another major advantage of our imaging-based aptasensing methodology is that it can simultaneously generate qualitative and quantitative readouts of cell viability in response to various treatments when cells are labeled with the appropriate detection dyes.

Regeneration of aptasensors

Moreover, the reusability of aptasensors were evaluated after regeneration treatment. As shown in the Figure S5, the florescence intensity detected from the regenerated Gr and rGO aptasensors immobilized either with Ap1 or Ap2 aptamer complexes were almost the same as that on the newly prepared aptasensors, signifying that the aptamer complex modified surface was not destroyed during regeneration treatment. The fluorescence signal was reduced by only 3.5% after 10 times of regeneration, which underlines the reusability of aptasensors. As shown in the Figure S6, the aptasensors have shown similar trend and the same limit of detection after the tenth regeneration which signifies the accuracy and reusability of regenerated aptasensors.

Conclusions

Small biomolecules play crucial roles in various physiological processes; thus, the quantitative detection of these molecules has become a topic of great interest. Here, we introduced a robust imaging-based, label-free approach to rapidly obtain quantitative readouts from aptasensors. Our rational integration of an imaging-based methodology with an image processing pipeline, which allows quantitative assessment through the subtraction of background and normalization of fluorescence signals, will potentially have a broad range of applications ranging from basic research to high-content drug screening. Moreover, our aptasensing quantification methodology does not require high-end microscopic instrumentation or specific techniques, making it suitable for the routine assessment of various biological entities. Although we focused the present study on carbon nanomaterials and drug screening, our methodology is universally applicable for the quantification of diverse biological targets including oligonucleotides, cells, hormones, enzymes, and small biomolecules. With the implementation of the appropriate cell culture system, our technique could also be adopted for simultaneous live/dead cell screening and biomolecule quantification in a high-throughput manner. Thus, the addition of a 3D cell culture system to our platform will enable efficacious drug screening with continuous dose-response monitoring. Moreover, changes in the biomolecule concentration can be calculated by determining the fluorescence intensities through image analysis.

Experimental

Chemicals

All chemicals, reagents, and oligonucleotides were purchased and used without further purification. Aptamers, including fluorescein amidite (FAM)-tagged versions thereof and their corresponding complementary sequences (cDNAs), were purchased from Integrated DNA Technologies, Inc. (IDT, Coralville, IA, USA) (**Table 1**).

Phosphate-buffered saline (PBS), 3-aminopropyltriethoxysilane (APTES), SYBR Green-I (SGI), and adenosine triphosphate (ATP) were purchased from Sigma-Aldrich (St. Louis, MO, USA), whereas 1-pyrenebutyric acid N-hydroxysuccinimide ester (PBASE) was purchased from Molecular Probes (Life Technologies, Gaithersburg, MD, USA). The HeLa cell line was obtained from the Korea Cell Line Bank (Seoul, Korea); RPMI 1640 medium was procured from Corning Inc., USA. 5-fluorouracil was purchased from Ameresco Co. (Solon, OH, USA) and doxorubicin and gemcitabine were purchased from Cayman Chemicals (Ann Arbor, MI, USA).

Table 1. Aptamers and their complementary DNA used in this study.

S. No.	Detail	Name	Sequence
1.	Aptamer 1	Ap1	5'-ACC TGG GGG AGT ATT GCG GAG GAA GGT-C_3-NH_2-3'
	Complementary sequence to Ap1		5'-ACC TTC CTC CGC AAT ACT CCC CCA GGT-3'
2.	Aptamer 2	Ap2	5'-TTT TTT TTA GTC TGG AAG GAG GCG TTA TGA GGG GGT CCA GAC TAT TTT TTT-C_3-NH_2-3'
	Complementary sequence to Ap2		5'-TGG ACC CCC TCA TAA CGC CTC CTT CCA GAC TAA AAA AAA-3'
3.	FAM labeled aptamer	Fap	5'-FAM- C_3-ACC TGG GGG AGT ATT GCG GAG GAA GGT-NH_2-3'
	Complementary sequence to Fap		5'-ACC TTC CTC CGC AAT ACT CCC CCA GGT-3'

Preparation of the substrates modified with 2D nanomaterials

The rGO-modified glass substrate was prepared as described elsewhere.[37] Briefly, the modified Hummer's method was used to synthesize graphite oxide (GO).[38] Layered GO was exfoliated, dispersed in water, and sonicated for 2 h to generate single-layer GO nanosheets. The sonicated GO solution was subsequently spun by centrifugation and the aqueous layer was discarded. The remaining GO was resuspended in water and used for all further procedures. Prior to the addition of GO, the glass substrates were cleaned and treated with 3% (3-aminopropyl)triethoxysilane (APTES), which promotes the formation of a positively charged surface through the addition of amine groups. The treated glass substrate was incubated with GO solution for 1 h and then washed thoroughly. To generate the rGO film, the immobilized GO substrate was reduced with hydrazine monohydrate (Alfa Aesar, Ward Hill, MA, 99.9% purity) at 60 °C for 12 h and then subjected to thermal annealing for 2 h at 200 °C.

Gr deposition and transfer were performed as in our recent study.[39] Briefly, the chemical vapor deposition (CVD) method was employed to deposit a single layer of Gr (25 µm thick) on Cu foil. A screen protector film was utilized to transfer the Gr sheet onto the substrate using the hydrogen bubbling method. Briefly, hydrogen bubbles were introduced in between the Gr sheet and the hydrophilic Cu foil, which released Gr from the Cu foil and allowed the Gr to attach onto the screen protector film. Later, the Gr on the screen protector film was carefully attached to the glass substrate. This step resulted in the transfer of Gr to the glass substrate due to its higher adhesion.

Aptamer immobilization

An equimolar mixture (1 µM) of the aptamers and their corresponding cDNA sequences was made in Tris buffer. The mixture was incubated at 90 °C for 5 min to denature all components and to prevent the formation of self-complementary or secondary structures, which interfere with the formation of dsDNA complexes (i.e., aptamer complexes). The mixture was then cooled to room temperature over 45 min and the resultant dsDNA were stored at 4 °C until further use. For label-free fluorescence-mediated ATP detection, 485 nM SGI solution was added to the dsDNA solution that had been prepared with either Ap1 or Fap. As expected, the higher was the concentration of SGI intercalated with the Ap2-cDNA due to a large number of oligonucleotides, the greater was the length of Ap2 required compared to Ap1. Here, 738 nM SGI solution was added to the dsDNA solution prepared with Ap2. The reactions were incubated for 10 min, thus allowing SGI to intercalate into the dsDNA molecules.

Subsequently, a 1-pyrenebutanoic acid succinimidyl ester (PBASE)-based method was used to covalently immobilize the aptamer complexes on the Gr and rGO surfaces as described elsewhere.[40] In this approach, the amine-reactive PBASE acts as a linker molecule between the aptamers and Gr/rGO. The PBASE linker molecules attach to the Gr surface through a π-π stacking mechanism. The Gr and rGO substrates were incubated with 10 mM PBASE in dry dimethylformamide for 1 h at RT to achieve functionalization. The substrates were then rinsed with dimethyl formamide (DMF), washed three times with PBS, and then washed with water.

For aptamer immobilization on glass substrate, the glass slides were cleaned with piranha solution (H_2SO_4:H_2O_2 in a 3:1 ratio) for 1 h and subsequently rinsed with DI water and dried in nitrogen flow. The glass substrates were then immersed in 2% (v/v) 3-aminopropyltriethoxysilane (APTES) in ethanol for 30 min at RT. The amine-modified substrates were then successively rinsed with ethanol and DI water and subsequently immersed in glutaraldehyde (2.5%) solution. The glass slides were kept in the solution for 1 h at room temperature and rinsed sequentially with DI water so as to eliminate all excess glutaraldehyde.

The aptamer complexes were added to the Gr, rGO and glass substrates and incubated overnight. In case of rGO and Gr, the terminal amine group of the aptamers reacts with the amine-reactive PBASE molecules, thus resulting in the formation of covalent bonds between PBASE molecules and the aptamers. Unbound aptamer complexes were removed from the substrates via a PBS wash. The modified substrate was then incubated with various concentrations of ATP and fluorescence images were recorded as described below.

Fluorescence microscopy image analysis and ATP quantification

For ATP quantification, a standard curve was first generated by incubating the Gr, rGO and glass aptasensors (immobilized with either Ap1 or Ap2 aptamer complexes) with a range of ATP concentrations (10^{-5} to 100 µM) for 20 min. Similarly, for intracellular ATP quantification, freshly prepared lysates of HeLa cells were added to the designated wells prior to imaging. Images were acquired after the appropriate incubation periods using a fluorescence microscope (Olympus, IX-81, Japan) equipped with a CCD camera and image acquisition software (Cellsense, Olympus). All images were recorded at the same pixel size. Images were analyzed using ImageJ software with the appropriate plugins (Wayne Rasband, National Institute of Health, Bethesda, MD, USA). Before calculating the fluorescence intensities, the width, height, and coordinates of a region of interest (ROI) were defined. The same dimensions were strictly used in the analysis of all other images. Pixel volumes at 5-40x magnification were calculated for each 1 µm of sample depth using the conversion factor 1000 L = 1 m^3. The overall mean changes in fluorescence intensity upon the addition of varying concentrations of ATP were calculated by spatially averaging the SGI fluorescence intensities. All images were recorded and stored in a preallocated system folder for offline processing. The control group consisted of Gr and rGO substrates without immobilized aptamer complexes, while the nontreated (NT) group consisted of Gr and rGO substrates that had been

immobilized with aptamer complexes before all experiments. These control and NT groups were used to correct variability due to auto fluorescence, imaging constraints, and minor equipment drift over time. Thus, these groups were important for ensuring accurate quantitative analysis of ATP concentrations. Furthermore, to assess the quenching capability of Gr and rGO and their role in significant background reduction, which can lead to accurate quantitative measurement, a comparative analysis of background signals was performed on glass substrate. Nonspecific signals on Gr, rGO and glass substrates were removed using background subtraction performed with the rolling-ball algorithm (Squassh protocol, MOSAIC). This algorithm removes all signals that cannot be accounted for after deconvolution and denoising of the quantitative measurements. The fluorescence intensity measurements were then rescaled and the mean fluorescence intensities were determined.

The addition of ATP induces the release of intercalated SGI from the aptamer complexes, resulting in a reduction of the fluorescence intensity. To quantify this reduction, the time required for ATP-aptamer interaction were first determined by plotting the fluorescence intensity over time. In subsequent experiments, the calibrated images were investigated for concentration-dependent changes in fluorescence.

As a control, the fluorescence intensities after the addition of various concentrations of ATP were quantified using an optical spectrophotometer (BioTek Synergy HT reader). These experiments were performed in 96-well plates and the volume was corrected for a 1 cm path length. Data were recorded at an excitation wavelength of 494 nm and an emission wavelength of 521 nm.

Intracellular ATP quantification

To demonstrate the efficacy of our strategy, we first validated the ability of the aptasensor approach to quantify intracellular ATP in the absence of any drug treatment, thus providing a viable cell count. To this end, HeLa cells were grown in culture flasks in RPMI 1640 medium supplemented with 10% FBS. Cells were incubated in a 5% CO_2 atmosphere at 37 °C and grown until reaching ~70% confluency. At this point, cells were detached with trypsin treatment. After detachment, fresh culture medium was added to deactivate the trypsin. Harvested cells were collected by centrifugation at 500 g for 5 min, washed twice with PBS, and then suspended in Tris buffer. The cells were then serially diluted to obtain cell suspensions ranging from 10^2 - 10^6 cells/ml and lysed by sonication. Cell lysates were then clarified by centrifugation at 500 g for 3 min at 4 °C. To avoid ATP hydrolysis by intracellular factors, all lysates were generated immediately before the start of each experiment. The supernatants were collected and immediately used in ATP assays as described above.

This ATP quantification method was also applied to a cytotoxicity assay. To this end, HeLa cells were treated with various concentrations of doxorubicin, 5-fluorouracil, and gemcitabine, which are commonly used in chemotherapy regimens. After treatment with these drugs, the intracellular ATP levels were quantified. Briefly, cells were grown in monolayers as described above, washed with PBS, and then incubated with drugs at the indicated concentrations (doxorubicin, 1-10 µM; 5-fluorouracil and gemcitabine, 0.01-5 µM) for 24 h. At the end of the incubation period, the intracellular ATP concentrations were immediately assessed.

As a control, drug-induced cytotoxicity was also analyzed by spectrometry. In this experiment, the fluorescence spectra of solutions containing either Ap1 or Ap2 complexes were recorded after 20 min of incubation with the cell lysates.

Aptasensor regeneration studies.

Following the imaging-based quantitative measurements using tunable platforms on different nanomaterials with ATP aptamers immobilized, wells were washed for 10 min in PBS followed by regeneration in new buffer. Regeneration was performed by soaking aptasensors in 10% SDS in 1x buffer for 10 min and then immersing in hot water followed by copious washing with double distilled water. After washing, the aptasensors were incubated with their respective complementary sequences overnight and then SGI solution was added to the dsDNA for the formation of aptamer complexes. The quantitative measurements were performed in the resulting regenerated aptasensors with the same procedure described above to analyze the fluorescence recovery.

Acknowledgements

This research was supported by the Basic Science Research Program (Grant No. 2010-0015035) through the National Research Foundation (NRF) of Korea, which is funded by the Ministry of Science, ICT, & Future Planning.

References

1. J. Capoulade, M. Wachsmuth, L. Hufnagel and M. Knop, *Nat. Biotechnol.*, 2011, **29**, 835–839.
2. H. Deschout, F. Cella Zanacchi, M. Mlodzianoski, A. Diaspro, J. Bewersdorf, S. T. Hess and K. Braeckmans, *Nat. Methods*, 2014, **11**, 253–66.
3. V. C. Coffman and J.-Q. Wu, *Mol. Biol. Cell*, 2014, **25**, 1545–8.
4. C.-G. Pack, H. Yukii, A. Toh-e, T. Kudo, H. Tsuchiya, A. Kaiho, E. Sakata, S. Murata, H. Yokosawa, Y. Sako, W. Baumeister, K. Tanaka and Y. Saeki, *Nat. Commun.*, 2014, **5**, 3396.
5. M. Wachsmuth, C. Conrad, J. Bulkescher, B. Koch, R. Mahen, M. Isokane, R. Pepperkok and J. Ellenberg, *Nat. Biotechnol.*, 2015, **33**, 384–389.
6. M. Lehmann, S. Rocha, B. Mangeat, F. Blanchet, H. Uji-i, J. Hofkens and V. Piguet, *PLoS Pathog.*, 2011, **7**.
7. N. Durisic, L. Laparra-Cuervo, Á. Sandoval-Álvarez, J. S. Borbely and M. Lakadamyali, *Nat. Methods*, 2014, **11**, 156–162.
8. M. Fritzsche and G. Charras, *Nat. Protoc.*, 2015, **10**, 660–680.
9. K. Abe, L. Zhao, A. Periasamy, X. Intes and M. Barroso, *PLoS One*, 2013, **8**, e80269.
10. K. Wang, A. Sachdeva, D. J. Cox, N. W. Wilf, K. Lang, S. Wallace, R. A. Mehl and J. W. Chin, *Nat. Chem.*, 2014, **6**, 393–403.
11. K. Okabe, N. Inada, C. Gota, Y. Harada, T. Funatsu and S. Uchiyama, *Nat. Commun.*, 2012, **3**, 705.
12. M. A. Yaseen, S. Sakadžić, W. Wu, W. Becker, K. A. Kasischke and D. A. Boas, *Biomed. Opt. Express*, 2013, **4**, 307–321.
13. J. C. Rohloff, A. D. Gelinas, T. C. Jarvis, U. A. Ochsner, D. J. Schneider, L. Gold and N. Janjic, *Mol. Ther. Acids*, 2014, **3**, e201.
14. W. Zhou, P.-J. J. Huang, J. Ding and J. Liu, *Analyst*, 2014, **139**, 2627–2640.
15. A. L. Chang, M. McKeague, J. C. Liang and C. D. Smolke, *Anal. Chem.*, 2014, **86**, 3273–3278.
16. X. Liu, L. Shi, X. Hua, Y. Huang, S. Su, Q. Fan, L. Wang and W. Huang, *ACS Appl. Mater. Inter.*, 2014, **6**, 3406–3412.

17. A. Shastri, L. M. McGregor, Y. Liu, V. Harris, H. Nan, M. Mujica, Y. Vasquez, A. Bhattacharya, Y. Ma and M. Aizenberg, *Nat. Chem.*, 2015, **7**, 447–454.
18. L. Li, Q. Wang, J. Feng, L. Tong and B. Tang, *Anal. Chem.*, 2014, **86**, 5101–5107.
19. Z. Zeng, C.-H. Tung and Y. Zu, *Mol. Ther. Acids*, 2014, **3**, e184.
20. T. Hianik, V. Ostatná, M. Sonlajtnerova and I. Grman, *Bioelectrochem*, 2007, **70**, 127–133.
21. M. Wu, R. Kempaiah, P.-J. J. Huang, V. Maheshwari and J. Liu, *Langmuir*, 2011, **27**, 2731–2738.
22. K. P. Loh, Q. Bao, G. Eda and M. Chhowalla, *Nat. Chem.*, 2010, **2**, 1015–1024.
23. A. Kasry, A. A. Ardakani, G. S. Tulevski, B. Menges, M. Copel and L. Vyklicky, *J. Phys. Chem. C*, 2012, **116**, 2858–2862.
24. M. S. Choi, M. Yoon, J.-O. Baeg and J. Kim, *Chem. Commun.*, 2009, 7419–7421.
25. A. I. Dragan, R. Pavlovic, J. B. McGivney, J. R. Casas-Finet, E. S. Bishop, R. J. Strouse, M. A. Schenerman and C. D. Geddes, *J. Fluoresc.*, 2012, **22**, 1189–1199.
26. H. Zipper, H. Brunner, J. Bernhagen and F. Vitzthum, *Nucleic Acids Res.*, 2004, **32**, e103–e103.
27. Y. He, X. Xing, H. Tang and D. Pang, *Small*, 2013, **9**, 2097–2101.
28. J. Liu, C. Wang, Y. Jiang, Y. Hu, J. Li, S. Yang, Y. Li, R. Yang, W. Tan and C. Z. Huang, *Anal. Chem.*, 2013, **85**, 1424–1430.
29. J.-J. Xu, W.-W. Zhao, S. Song, C. Fan and H.-Y. Chen, *Chem. Soc. Rev.*, 2014, **43**, 1601–1611.
30. M. N. Stojanovic, P. De Prada and D. W. Landry, *J. Am. Chem. Soc.*, 2001, **123**, 4928–4931.
31. M. N. Stojanovic, P. de Prada and D. W. Landry, *J. Am. Chem. Soc.*, 2000, **122**, 11547–11548.
32. B. Kim, I. H. Jung, M. Kang, H.-K. Shim and H. Y. Woo, *J. Am. Chem. Soc.*, 2012, **134**, 3133–3138.
33. J. Zhang, L. Wang, H. Zhang, F. Boey, S. Song and C. Fan, *Small*, 2010, **6**, 201–204.
34. Y. Zhang, Y. Wang and B. Liu, *Anal. Chem.*, 2009, **81**, 3731–3737.
35. T. Qiu, D. Zhao, G. Zhou, Y. Liang, Z. He, Z. Liu, X. Peng and L. Zhou, *Analyst*, 2010, **135**, 2394–2399.
36. C.-H. Lu, X.-J. Qi, J. Li and H.-H. Yang, in *Aptamers Selected by Cell-SELEX for Theranostics*, Springer, 2015, pp. 163–195.
37. I.-Y. Sohn, D.-J. Kim, J.-H. Jung, O. J. Yoon, T. N. Thanh, T. T. Quang and N.-E. Lee, *Biosens. Bioelectron.*, 2013, **45**, 70–76.
38. N. I. Kovtyukhova, P. J. Ollivier, B. R. Martin, T. E. Mallouk, S. A. Chizhik, E. V Buzaneva and A. D. Gorchinskiy, *Chem. Mater.*, 1999, **11**, 771–778.
39. W.-I. Lee, I.-Y. Sohn, B. Y. Kim, Y.-M. Son, J.-H. Shin, H.M. Kim, Y.J. Suh, N.-E. Lee, *Sci. adv. Mater.* 2015**, 7**, 1540-1545.
40. Y. Ohno, K. Maehashi, K. Inoue and K. Matsumoto, *Jpn J Appl Phys*, 2011, **50**, 70120.